Charge-transfer complexes from decamethylferrocene and 1,4-quinone derivatives: neutral-ionic phase diagrams for metallocene complexes.

Mochida, Tomoyuki

Funasakoa, Yusuke

Azumi, Hiroko

(Citation)
Dalton transactions,40:9221-9228

(Issue Date)
2011-09-28

(Resource Type)
journal article

(Version)
Accepted Manuscript

(URL)
https://hdl.handle.net/20.500.14094/90001806

Charge-transfer Complexes from Decamethylferrocene and 1,4-Quinone Derivatives — Neutral–ionic Phase Diagrams for Metallocene Complexes†

Tomoyuki Mochida,[a,b] Yusuke Funasako[a] and Hiroko Azumi[b]

Charge-transfer (CT) complexes of ferrocenes with 1,4-quinone derivatives were investigated. Deca- and octamethylferrocene complexes with 1,4-naphthoquinone derivatives were prepared and structurally characterized; these were neutral 1:2 DA complexes with mixed-stack structures. The formation of complexes with 1,4-benzoquinones was examined by applying solvent-drop grinding. CT energies and phase transitions in these neutral and other ionic complexes were investigated. Their electronic states are discussed on the basis of the phase diagrams derived for mixed-stack ferrocene-based CT complexes, taking into account their dependence on the DA ratio, dimensionality, and intermolecular interactions.

---

[a]*Department of Chemistry, Graduate School of Science, Kobe University, Rokkodai, Nada, Hyogo 657-8501, Japan.*
E-mail: tmochida@platinum.kobe-u.ac.jp
[b]*Department of Chemistry, Faculty of Science, Toho University, Miyama, Funabashi, Chiba 274-8510, Japan*

†Electronic supplementary information (ESI) available: TG traces of **1** and **2** (Fig. S1), XRD patters of powders obtained by ball-milling of $[Fe(C_5HMe_4)_2]$ and Cl_2BQ (Fig. S2), solid-state electronic spectra of $[Fe(Cp^*)_2][TCNQ]$, $[Fe(C_5HMe_4)_2][TCNQ]$, and $[Fe(Cp^*)_2][DMDCNQI]$ (Fig. S3), solid-state electronic spectra of $[Co(Cp^*)_2]$ salts (Fig. S4), and DSC trace for $[Fe(Cp^*)_2][TCNQ]$ (1-D phase) and $[Fe(C_5HMe_4)_2][TCNQ]$ (Fig. S5). CCDC reference numbers 766109 (**1**), 766110 (**2**), and 766111 (**3**). See DOI: 10.1039/xxxxxxxx

Introduction

Metallocene-based charge-transfer (CT) complexes have attracted special attention from the viewpoint of molecular magnetism.[1,2] In particular, decamethylferrocene ([Fe(Cp*)$_2$]) affords a variety of CT complexes that are magnetically interesting.[3,4] Among them, the best-studied example is [Fe(Cp*)$_2$][TCNE], which exhibits ferromagnetic ordering below 4.8 K.[5] To date, many ferrocene-based CT complexes have been synthesized; most are ionic complexes, such as those with $TCNQ^{\cdot -}$, metal-dithiolates, and other anions.[1–6] Our continuous investigations into phase transitions in ferrocene-based materials have also focused on ionic materials.[7] Thus, although neutral CT complexes have drawn less attention, it is expected that neutral metallocenium complexes will exhibit neutral–ionic (NI) transitions[8] if the redox potentials of the components are suitable. The NI transitions are observed in organic CT complexes such as tetrathiafulvalene–chloranil, and have attracted special attention.[9,10] This is a transition from a neutral state (D^0A^0) to an ionic state (D^+A^-) at low temperatures or under high pressures, which is characteristic of neutral mixed-stack CT complexes located near the NI boundary. The boundary is located where the difference of the redox potentials between the donor and the acceptor (ΔE_{redox}) is approximately 0.2 V. NI phase diagrams plotted against ΔE_{redox} have been examined for various organic CT complexes.[9,11] In addition to planar organic molecules, C_{60} also affords ionic and neutral complexes with donors including metallocenes,[12] and their ionicity has been discussed.[13] However, the NI phase boundary as well as the possibility of the transition for metallocene complexes has received less attention.[8] Metallocenes tend to form mixed-stack CT complexes, which are suitable for a NI transition, and the transition is expected to accompany a magnetic change as a result of the suppression of Peierls instability in the ionic phase.

As a basic study in search of NI transitions in metallocene-based CT complexes, we focused on complexes of decamethylferrocene ([Fe(Cp*)$_2$]) and octamethylferrocene ([Fe(C_5HMe_4)$_2$]) with planar organic acceptors. In the ionic region, several mixed-stack complexes of decamethylferrocenes are known, such as [Fe(Cp*)$_2$][TCNQ] (1-D phase),[14] [Fe(C_5HMe_4)$_2$][TCNQ],[15] and [Fe(Cp*)$_2$][DMDCNQI] (DMDCNQ = *N*,*N*′-dicyano-2,5-dimenthyl-1,4-benzoquinonediimine).[16] In contrast, very few neutral complexes are known, such as [Fe(Cp*)$_2$][acenaphthenequinone].[17] In search of neutral complexes, we used quinone derivatives, which are weaker acceptors than TCNQ and DMDCNQI, whereas [Fe(Cp*)$_2$][2,3-dicyano-1,4-naphthoquinone] is an ionic complex.[18] First, we used naphthoquinones to

prepare [Fe(Cp*)$_2$][2,3-dichloro-1,4-naphthoquinone]$_2$ (**1**), [Fe(Cp*)$_2$][2,3-dibromo-1,4-naphthoquinone]$_2$ (**2**), and [Fe(C$_5$HMe$_4$)$_2$][2,3-dichloro-1,4-naphthoquinone]$_2$ (**3**) (Figure 1), and structurally characterize them. Second, the formation of complexes with benzoquinone (Figure 2) was investigated by applying solid-state reactions. Third, the CT bands in these neutral complexes and the known ionic complexes[14–16] were evaluated. NI phase diagrams for ferrocene-based CT complexes were derived, and their dependence on the DA ratio, dimensionality, and intermolecular interactions were examined. The electronic states of the complexes are discussed on the basis of the diagrams. In addition, phase transitions in these complexes were investigated by differential scanning calorimetry (DSC) measurements.

Results and Discussion

Crystal structures of naphthoquinone complexes 1–3.

Complexes **1**–**3** were obtained as dark red prismatic crystals through the slow evaporation of acetone or dichloromethane solutions of the components. These complexes were isomorphous and exhibited a 1:2 DA ratio. The packing diagrams of **2** are presented in Figure 3. The donors and pairs of acceptors are stacked alternately along the *a*-axis. The Cp* rings in the donors have a staggered conformation, and the rings contact the quinone six-membered ring of the acceptor. In **3**, the eight methyl groups of octamethylferrocene are disordered over ten sites with a 0.8 occupancy, appearing like decamethylferrocene.

These were neutral complexes, as expected from the weak electron affinities of the acceptors. The average Fe–C(Cp) distances in the donor molecules of **1**–**3** are 2.050 Å, 2.053 Å, and 2.049 Å, respectively, which are comparable to those in decamethylferrocene (2.050 Å)[19] and octamethylferrocene (2.054 Å)[20]. Intramolecular Cp–Cp centroid distances are 3.306 Å, 3.316 Å, and 3.313 Å, respectively. The bond lengths of the acceptors (1.211–1.215 Å) are comparable to those observed in 2,3-dichloro-1,4-naphthoquinone (1.205 Å).[21,22] Consistently, C=O stretching vibrations in the infrared spectra of **1** (1678 cm^{-1}), **2** (1672 cm^{-1}), and **3** (1679 cm^{-1}) appeared at almost the same frequency as those of 2,3-dichloro-1,4-naphthoquinone (1680 cm^{-1}) and 2,3-dibromo-1,4-naphthoquinone (1672 cm^{-1}). Therefore, the degree of CT is only slight in these complexes. This is probably ascribed to the small overlap integrals between the donor and the acceptor as a result of the localization of the highest-occupied molecular orbital (HOMO) of the donor on the Fe atom, in addition to the difference of the redox potentials.

The crystallographic parameters of **1**–**3** are listed in Table 1, the comparison of which is interesting from the viewpoint of chemical pressure. The cell volume of **2** (1798.0(3) Å^3) is larger than that of **1** (1738.1(2) Å^3) by 3.5%, where lengthening of the *c*-axis (+1.7%) is the most significant change among the axes, consistent with the arrangement of the acceptor. A comparison of the unit cell volumes of **1** and **3** (1699.5(6) Å^3) reveals that the latter is 2.2% smaller, despite the disordered molecular structure of octamethylferrocene. By changing the substituents, the cell volumes were controllable by ca. 5% in total. Intermolecular distances between the centroid of the Cp* ring of the donor and the acceptor plane are 3.613 Å (for **1**), 3.518 Å (for **2**), and 3.495 Å (for **3**), indicating a shortening of the donor–acceptor distance in **3**. Interplane distances between the acceptors within the pairs are 3.424 Å (for **1**), 3.459 Å (for **2**), and 3.436 Å (for **3**).

Charge-transfer bands in 1–3. CT bands of these complexes appeared at around 600–800 nm. The UV-vis-NIR absorption spectra of powder samples of **1** and its components are depicted in Fig. 4. The absorption maxima of the CT bands were observed at 627 nm (1.98 eV) and 637 nm (1.94 eV) for **1** and **2**, respectively. The overlap integrals between the lowest-unoccupied molecular orbitals (LUMO) of the acceptors in the acceptor pair were calculated to be very small, 1.52×10^{-3} (for **1**), 1.70×10^{-3} (for **2**), and 1.60×10^{-3} (for **3**), which suggests that the interactions are negligible. Therefore, the CT occurs from the donor to the adjacent acceptor, nearly independently of the other acceptor within the pair.

Phase transitions and thermal properties of 1–3

DSC measurements revealed that **3** undergoes a first-order phase transition, whereas no phase transitions were observed in **1** and **2**. The transition occurred at 155.8 K (ΔS = 2.0 J K^{-1} mol^{-1}), accompanying thermal hysteresis of ΔT = 18.5 K (Table 2). To investigate the origin of the phase transition, we collected X-ray diffraction data at 90 K to find that a superlattice structure is formed in the low temperature phase. The *a*- and *b*-axes at 90 K were three times longer than those in the room temperature phase: *a* = 40. 95 Å, *b* = 24.51 Å, *c* = 15.05 Å^3, β = 96.65°, *V* = 15122 Å^3. Preliminary analysis revealed that slight canting of the molecular orientation, which may be possibly related to the ordering of the methyl group in **3**, causes the superlattice structure. Tripling of the unit cell associated with a phase transition is interesting and detailed structural analyses will be reported elsewhere.

DSC measurements revealed that **1** and **2** melted at 450.5 K and 465.4 K, respectively, which was

immediately followed by decomposition. **3** melted at 426.2 K with only a slight decomposition, associated with a melting entropy of ΔS = 146 J K^{-1} mol^{-1} and a hysteresis of ΔT = 17.3 K (Table 2). The lower melting point of **3** is ascribable to the lower symmetry of the donor. Thermogravimetric analysis (TG) of **1** and **2** revealed that their melting accompanies a sudden weight loss corresponding to the decomposition observed in DSC (Figure S1, supporting information). Weight loss of approximately 15% occurred for **1** at around 450 K, and weight loss of approximately 25% occurred for **2** at around 470 K, after which gradual weight losses continued.

Formation of benzoquinone complexes by solid-state reactions

Complexes of metallocenes with benzoquinones were not formed from solution reactions. Therefore, the formation of complexes by means of solvent-drop grinding[23] was investigated, because solid-state reactions are known to be effective for the preparation of CT complexes from benzoquinones.[24] Thus, fluoranil (F_4BQ), chloranil (Cl_4BQ), bromanil (Br_4BQ), and 2,5-dichlorobenzoquinone (Cl_2BQ) with [M(Cp*)$_2$] (M = Fe, Co) or [Fe(C_5HMe_4)$_2$] were mixed and subjected to grinding after adding a drop of dichloromethane. In all cases, color changes were observed by grinding. [Fe(Cp*)$_2$] and [Fe(C_5HMe_4)$_2$] produced brown or green powders, whereas [Co(Cp*)$_2$] produced dark brown powders. In their UV-vis spectra, broad bands assignable to CT bands were observed. Products from [Fe(Cp*)$_2$] and [Fe(C_5HMe_4)$_2$] exhibited a band at around 750−780 nm (~1.6 eV), whereas those from [Co(Cp*)$_2$] exhibited a CT band at around 460−590 nm (2.1−2.7 eV) as a shoulder (Figure S4). Absorption spectra for the reaction products of [Fe(Cp*)$_2$] or [Fe(C_5HMe_4)$_2$] with [X_4BQ] (X = Cl, Br) are depicted in Figure 5. λ_{max} of the CT bands are listed in Table 3, together with the redox potentials of their components. The CT bands in the products of [Fe(Cp*)$_2$] appeared at slightly higher energies (0.05 eV higher) than those from [Fe(C_5HMe_4)$_2$], consistent with the difference in the redox potentials of the donors.

By measuring X-ray diffraction (XRD) patterns, the formation of bulk CT complexes was investigated. Of the twelve combinations, solvent-drop grinding produced bulk 1:2 DA complexes of [Fe(C_5HMe_4)$_2$][Cl_4BQ]$_2$, [Fe(C_5HMe_4)$_2$][Cl_2BQ]$_2$, and [Fe(Cp*)$_2$][Cl_2BQ]$_2$, for which new XRD peaks appeared. The reaction proceeded more efficiently by applying ball-milling. For [Fe(C_5HMe_4)$_2$][Cl_2BQ]$_2$, ball-milling with a DA mixing ratio of 1:2 in the presence of a drop of dichloromethane produced a single component assignable to a

CT complex, whereas an excess donor remained for a mixing ratio of 1:1 (Figure S2, supporting information). Similar results were observed for $[Fe(C_5HMe_4)_2][Cl_4BQ]_2$ and $[Fe(Cp^*)_2][Cl_2BQ]_2$, though the reactions were less efficient. In their infrared (IR) spectra, no shift of C=O stretching vibrations of the acceptors was observed, indicating that the degree of CT is negligible. Therefore, these complexes are neutral and probably have mixed-stack structures, although their structures are unknown. Combinations that produce bulk CT salts by grinding were thus fewer, and for the other nine combinations, no new XRD peaks were observed after grinding, whereas F_4BQ produced amorphous. The CT absorptions observed for them likely occur from the complexes formed on surfaces and in defects.

CT bands and phase transitions in ionic CT complexes

To investigate CT transitions in ionic complexes, we evaluated CT bands in $[FeCp^*_2][TCNQ]$ (1-D phase),[14] $[Fe(C_5HMe_4)_2][TCNQ]$[15] and $[Fe(Cp^*)_2][DMDCNQI]$[16]. CT bands for the TCNQ and DCNQI complexes were observed at around 680 and 880 nm, respectively (Table 4 and Figure S3, supporting information). In addition, phase transitions were investigated by DSC measurements, which revealed that $[FeCp^*_2][TCNQ]$ and $[Fe(C_5HMe_4)_2][TCNQ]$ exhibit first-order phase transitions (Table 2 and Figure S5, supporting information). $[Fe(C_5HMe_4)_2][TCNQ]$ exhibited a phase transition at 395.4 K (ΔS = 19.4 J K^{-1} mol^{-1}) with a hysteresis of ΔT = 4.8 K. Although structure determination at high temperature was not possible, the transition is probably correlated with a rotational disorder of the methyl groups, considering the disordered structure found in **3**. Consistently, $[FeCp^*_2][TCNQ]$ (1-D phase) did not exhibit phase transitions at high temperatures. Indeed, the disordering of four methyl groups to five sites in the molecule accompanies an entropy change of $\Delta S = 2R \ln 5$ = 26.7 J K^{-1} mol^{-1}, which is consistent with the observed value. At low temperatures, both $[FeCp^*_2][TCNQ]$ and $[Fe(C_5HMe_4)_2][TCNQ]$ exhibited phase transitions with small entropy changes at 215.9 K (ΔS = 3.0 J K^{-1} mol^{-1}, thermal hysteresis ΔT =1.7 K) and 226.5 K (ΔS = 1.2 J K^{-1} mol^{-1}, thermal hysteresis ΔT = 44.8 K), respectively. These transitions are probably associated with slight structural changes. No phase transition was observed in $[Fe(Cp^*)_2][DMDCNQI]$ in the measured temperature range of −150–100°C.

NI phase diagrams for ferrocene-based complexes

In the following sections, we extend the NI phase diagram derived by Torrance[9] for organic CT complexes to ferrocene-based CT complexes. The CT energies ($h\nu$) of mixed-stack CT complexes are generally given by $h\nu_{\mathrm{neutral}} = I_{\mathrm{D}} - E_{\mathrm{A}} - V$ and $h\nu_{\mathrm{ionic}} = (2\alpha - 1)V - (I_{\mathrm{D}} - E_{\mathrm{A}})$, for neutral and ionic complexes, respectively,[9] where I_{D} is the ionization energy of the donor, E_{A} is the electron affinity of the acceptor, α is the Madelung constant, and $V = 1/(4\pi\varepsilon\varepsilon_0 d)$ is the Coulomb energy, where d is a distance between the donor and the acceptor. $I_{\mathrm{D}} - E_{\mathrm{A}}$ is related to $\Delta E_{\mathrm{redox}}$ by $I_{\mathrm{D}} - E_{\mathrm{A}} = \Delta E_{\mathrm{redox}} + \Delta G$, where ΔG is a solvation energy.[9] In ferrocene-based complexes, because the intramolecular Cp–Cp distance in the donor is comparable to the π–π stacking distance,[7a,35] the donor–acceptor distance (d') becomes larger than those in organic complexes (d), as schematically depicted in Figure 6: $d' = 3/2d$ for 1:1 complexes and $d' = 2d$ for 1:2 complexes. CT energies in the ionic region depend on the dimensionality of the electrostatic interaction as well as the Madelung constant α. Three-dimensional (3D) systems should be considered for ferrocene-based systems, whereas organic mixed-stack CT complexes can be regarded as mostly one-dimensional (1D). In contrast to organic CT complexes, partial CT does not occur in metallocene complexes because of the localization of HOMO on the metal atom; hence, this simple model would provide a reasonable picture. In the following, phase diagrams for the 1:1 and 1:2 DA complexes are discussed separately.

Phase diagram for 1:1 complexes

Theoretical lines representing the correlations between the CT energies and $\Delta E_{\mathrm{redox}}$ for 1D and 3D 1:1 ferrocene complexes, as obtained based on the above consideration, are drawn in Figure 7a, together with that for conventional organic CT complexes. The CT energies in the ionic region depend on dimensionality, whereas they are the same in the neutral region. Values of α = 1.38 and 1.76, which are the values for ideal 1D and the cesium chloride structure, were used here for 1D and 3D, respectively. The NI boundaries are located at the intersections of the neutral and ionic lines in Figure 7a, where $\Delta E_{\mathrm{redox}}$ are –0.76 V and 0.10 V, for 1D and 3D, respectively. The boundary for 1D ferrocene complexes is located approximately 1 V to the negative side compared with that for the conventional complexes because of the reduction of Madelung gain in the ionic phase. The NI boundary moves to the right when the dimensionality is increased to 3D.

The CT energies in the 1:1 ionic complexes [Fe(Cp*)$_2$][TCNQ] (1D phase), [Fe(C$_5$HMe$_4$)$_2$][TCNQ], and

[Fe(Cp*)$_2$][DMDCNQI] (Table 4) are plotted versus ΔE_{redox} in the figure, which fall on the 1:1 theoretical line. Considering that they are ionic complexes, the plot indicates that the phase boundary for the 1:1 complexes is closer to the 3D one, which is ascribable to the long-range character of the electrostatic interaction. This is in contrast with magnetic interactions, which can become 1D in ferrocene complexes,[5] operating via π–π contacts. It is noteworthy that the DMDCNQI complex is located very close to the NI boundary, but the transition to a neutral phase was not found in the measured temperature range. We have also demonstrated the usefulness of this plot in understanding the electronic structures of relevant methylferrocene-DCNQI complexes.[36]

Phase diagram for 1:2 complexes

To obtain a neutral-ionic phase diagram for mixed-stack 1:2 ferrocene complexes, the interaction between the acceptors within the pairs should be taken into account. A diagram is presented in Figure 7b, which shows the theoretical correlations that correspond to cases of small and large interactions within the pair.

When the interaction is negligible, CT occurs from the donor to the adjacent acceptor with $d' = 3/2d$ (Figure 6b), which is the case for **1**–**3**. The CT energies in the neutral region become identical to those for the 1:1 complexes. The situation, however, becomes different in the ionic region; charge separation occurs in the acceptor pair (...$D^+A^-A^0D^+A^-A^0$...) owing to the small interaction. The Madelung constant for this 1D charge arrangement is $\alpha = 1.526$, which can be obtained by simple summation of the electrostatic interactions. The values of α for higher dimensions are usually difficult to obtain. We numerically obtained the value of $\alpha = 1.344$ for 3D based on the crystal structure of **1**, assuming point-charges on the Fe atom of the donor and on the acceptor pair. The 3D value was found to be smaller than the 1D value for these charge arrangements. These values were used to derive the correlations of $h\nu$ with ΔE_{redox} in the ionic region, which are the lines indicated by small *S* in Figure 7b. The plots for the 1:2 naphthoquinone complexes **1**–**3** fall on the neutral line. The use of stronger donors such as [M(Cp*)$_2$] (M = Mn, Co) would afford complexes closer to the boundary. Plots for the 1:2 benzoquinone complexes [Fe(C$_5$HMe$_4$)$_2$][Cl$_4$BQ]$_2$, [Fe(C$_5$HMe$_4$)$_2$][Cl$_2$BQ]$_2$, and [Fe(Cp*)$_2$][Cl$_2$BQ]$_2$, which again fall on the neutral line, are presented in the figure. Other reaction products of benzoquinones are located nearby. Therefore, both the 1:2 complexes of naphthoquinones and benzoquinones are located in the neutral region, away from the boundary. However, if these components

form 1:1 complexes, they will be located very close to the boundary, considering Figure 7a. Therefore, the preparation of 1:1 complexes of ferrocene derivatives with quinones will be a hopeful target in the search for NI transitions. In Figure 7b, CT energies for the reaction products of [Co(Cp*)$_2$] and benzoquinones are plotted tentatively (gray circles), although no crystalline complexes were obtained. The plot indicates that the products are ionic, as expected from the redox potentials.

When the interaction between the acceptors is sufficiently large, accompanying dimerization, CT occurs from the donor to the acceptor dimer with $d' = 2d$ (Figure 6c), and the charge distribution in the ionic region becomes uniform (...$D^{+}A^{-0.5}A^{-0.5}D^{+}A^{-0.5}A^{-0.5}$...). Therefore, theoretical lines in both the N and I regions are derived solely by changing the donor–acceptor distance (Figure 7b, lines indicated by large *S*). In this case, the effective redox potential of the acceptor is lowered by dimerization, which would affect $\Delta E_{\mathrm{redox}}$ and the NI boundary by 0.1–0.2 V, considering the usual values of transfer integrals in organic compounds. This was not considered in the plot because the effect is small and dependent on materials.

Conclusion

Neutral 1:2 CT complexes were formed by reactions of deca- and octamethylferrocenes with naphthoquinone and benzoquinone derivatives. Neutral-ionic phase diagrams for mixed-stack ferrocene-based CT complexes were derived, which correlate with the CT energies and redox potentials of the components. CT energies observed in the neutral 1:2 complexes and known ionic 1:1 mixed-stack complexes are in good agreement with the diagram. Several first-order phase transitions were found for the complexes, although they were not NI transitions. Tripling of the unit cell axes was found associated with the phase transition at low temperature in an octamethylferrocene complex. As we have demonstrated for relevant complexes,[36] the diagrams derived here are helpful in the search for NI transitions in metallocene-based CT complexes. The possibilities of NI transitions in these and related complexes are under investigation in our laboratories.

Experimental

General

Infrared spectra were recorded as KBr pellets on a Thermo Nicolet Avatar 360 spectrometer. Solid-state

electronic spectra were measured on a JASCO V-570 UV/VIS/NIR spectrometer equipped with an integrating sphere for diffuse reflectance spectroscopy, and the Kubelka–Munk conversion was applied to the resultant spectra. The spectra for solid-state reaction products were obtained by the use of KBr pellets. DSC measurements were performed using a Q100 differential scanning calorimeter (TA Instruments) in the temperature range 100–450 K at a rate of 10 K min^{-1}, and the data were averaged over a few cycles. TG analysis was performed under a nitrogen atmosphere at a heating rate 10 K min^{-1} on a Seiko TG/DTA 220U. Intermolecular overlap integrals were calculated by the extended Hückel molecular orbital method using a software package developed by Professor Mori (Tokyo Institute of Technology).[37] The molecular coordinate data obtained by X-ray structure determination was used for the calculation.

Materials

DMDCNQI (*N*,*N*′-dicyano-2,5-dimenthyl-1,4-benzoquinonediimine) was prepared according to the literature.[38] Other chemicals were commercially available. **1** was obtained as dark red prismatic crystals through the slow evaporation of acetone or dichloromethane solutions of equimolar amounts of the donor and acceptor at room temperature. Anal. Calcd. for $C_{40}H_{38}Cl_4FeO_4$ (780.35): C, 61.56; H, 4.91, Found: C, 61.52; H, 5.10. **2** was obtained by a similar procedure from a dichloromethane solution at −50 °C. Anal. Calcd. for $C_{40}H_{38}Br_4FeO_4$ (958.19): C, 50.14; H 4.00, Found: C, 50.01; H, 4.08. **3** was obtained by a similar procedure from an acetone solution at room temperature in a very low yield. These crystals, **3** in particular, gradually deteriorated at room temperature under air. The reaction of octamethylferrocene with dibromonaphthoquinone did not afford CT complexes. [$FeCp^*_2$][TCNQ] (1-D phase),[14] [$Fe(C_5HMe_4)_2$][TCNQ],[15] and [$FeCp^*_2$][DMDCNQI][16] were obtained by recrystallization from acetonitrile and identified by measuring XRD.

Solid-state reactions

A mixture of metallocenes and benzoquinones in a molar ratio of 1:1 or 1:2 were ground in the presence of a drop of dichloromethane in agate and mortar for 5 min. Experiments for [$CoCp^*_2$] were carried out under a nitrogen atmosphere. The reactions were also carried out by ball-milling using a Fritsch P-7 planetary mill with the aid of zirconia beads (750 rpm, 15 min). After the grinding, the products were thoroughly dried in

vacuum.

X-ray structure determination

XRD data for single crystals were collected on a Bruker SMART APEX II CCD diffractometer, using Mo Kα radiation (λ = 0.71073 Å). Crystal data, data collection parameters, and analysis statistics for these compounds are listed in Table 1. All calculations were performed using SHELXL.[39] The nonhydrogen atoms were anisotropically refined, and hydrogen atoms were inserted at calculated positions. Empirical absorption corrections (SADABS[40]) were applied. Disordered methyl groups of C_5Me_4H in donor molecule of **3** were placed in five sites with 0.8 occupancies. The packing diagrams were drawn using ORTEP-3.[41] CCDC 766109 (**1**), 766110 (**2**), and 766111 (**3**). contain the supplementary crystallographic data for this paper. These data can be obtained free of charge from the Cambridge Crystallographic Data Centre via www.ccdc.cam.ac.uk/data_request/cif.

Acknowledgments

We thank Professor T. Uchino for his help with ball-milling experiments and Professor Y. Harima (Department of Physics, Kobe University) for the calculation of Madelung constants. We also thank Y. Murao for the preparation of benzoquinone complexes and T. Akasaka for his help with crystallographic analysis. This work was financially supported by a Grant-in-Aid for Scientific Research (No. 23110719) from the JSPS (Japan Society for the Promotion of Science). We are grateful to M. Nakama (WarpStream Ltd., Tokyo) for providing a web-based database system. We also thank the anonymous reviewers for their valuable comments on the crystal structures and phase transitions.

Figure Caption

Fig. 1 Chemical formulas of complexes **1**–**3**.

Fig. 2 Chemical formulas of metallocene–benzoquinone complexes.

Fig. 3 Packing diagrams of **2** viewed from (a) *b*-axis and (b) *a*-axis. Hydrogen atoms are omitted for clarity.

Fig. 4 UV-vis-NIR spectra of [FeCp*$_2$][2,3-dichloro-1,4-naphthoquinone]$_2$ (**1**) (solid line), [FeCp*$_2$] (dotted line), and 2,3-dichloro-1,4-naphthoquinone (dashed line) in the solid state.

Fig. 5 UV-vis-NIR spectra of powders prepared by solvent-drop grinding of (a) [Fe(Cp*)$_2$] and Cl_4BQ, (b) [Fe(C_5HMe_4)$_2$] and Cl_4BQ, (c) [Fe(Cp*)$_2$] and Br_4BQ, and (d) [Fe(C_5HMe_4)$_2$] and Br_4BQ.

Fig. 6 Schematic illustration depicting the donor–acceptor distances in mixed-stack CT complexes. (a) Complexes from planar organic molecules, (b) 1:1 ferrocene-based complexes, and (c) 1:2 ferrocene-based complexes.

Fig. 7 Correlations between ΔE_{redox} and CT transition energies in mixed-stack CT complexes. (a) Diagram for 1:1 CT complexes. Theoretical correlations for ferrocene-based complexes and planar organic complexes are represented by solid lines and dashed lines, respectively. Correlation for 1D in ferrocene-based complexes is represented by the dotted line. Plots for [Fe(Cp*)$_2$][DMDCNQI] (open triangle), [Fe(Cp*)$_2$][TCNQ], and [Fe(C_5HMe_4)$_2$] [TCNQ] (open squares) are shown. (b) Diagram for 1:2 complexes. Theoretical correlations for complexes with small and large interactions within the acceptor pairs are represented by black lines (small *S*) and gray lines (large *S*), respectively. Correlations for 1D are represented by the dotted line. Plots for **1** and **2** (open circles), 1:2 complexes with benzoquinones (filled circles), and [Co(Cp*)$_2$]–benzoquinone grinding products (shaded circles) are shown.

Table 1. Crystallographic parameters for **1**, **2** and **3**

	1	**2**	**3**
Formula	C40 H38 Cl4 Fe O4	C40 H38 Br4 Fe O4	C38 H34 Cl4 Fe O4
Formula weight	780.35	958.19	750.29
T / K	173	173	173
Crystal system	Monoclinic	Monoclinic	Monoclinic
Space group	$P2_1/c$	$P2_1/c$	$P2_1/c$
a / Å	13.8780(10)	14.0046(12)	13.8846(3)
b / Å	8.3613(6)	8.4462(7)	8.1681(17)
c / Å	15.0171(10)	15.2741(13)	15.110(3)
β / deg	94.092(2)	95.6160(10)	96.016(2)
V / Å^3	1738.1(2)	1798.0(3)	1699.5(3)
Z	2	2	2
D_{calc} / g cm^{-3}	1.491	1.77	1.466
μ / mm^{-1}	0.784	4.906	0.799
Reflections collected	12597	9336	9312
F(000)	808	952	772
Parameters	244	228	228
Final R_1[a], wR_2[b] ($I > 2\sigma$)	0.0486, 0.1067	0.0214, 0.0536	0.0376, 00988
Final R_1[a], wR_2[b] (all data)	0.0603, 0.1121	0.0262, 0.0552	0.0451, 0.1039
Goodness of fit on F^2	1.094	1.077	1.048

[a] $R_1 = \Sigma \, ||F_o| - |F_c|| \, / \, \Sigma \, |F_o|$, [b] $wR_2 = [\, \Sigma \, w(F_o^2 - F_c^2)^2 \, / \, \Sigma \, w(F_o^2)^2 \,]^{1/2}$

Table 2. DSC data for ferrocene-based CT complexes

	Heating run			Cooling run			
	T (K)	ΔH (kJmol^{-1})	ΔS (JK^{-1}mol^{-1})	T (K)	ΔH (kJmol^{-1})	ΔS (JK^{-1}mol^{-1})	ΔT (K)
[Fe(C_5HMe_4)$_2$][Cl_2-naphthoquinone] (**3**)	174.6	0.46	2.65	155.1	0.59	3.83	19.5
	426.2[a]	63.0	146.05	408.9	9.63[b]	23.94[b]	17.3
[Fe(Cp*)$_2$][TCNQ] (1-D phase)	215.9	0.66	3.02	214.2	0.61	2.90	1.7
[Fe(C_5HMe_4)$_2$][TCNQ]	226.5	0.28	1.23	181.7	0.24	1.33	44.8
	395.4[a]	7.70	19.4	390.6	7.52	19.4	4.8

[a] Melting. [b] Smaller due to decomposition.

Table 3. Redox potentials of ferrocenes and quinones, and CT energies observed in powders obtained by solvent-drop grinding.

Donor	Acceptor	E_D / V[a)]	E_A / V[a)]	ΔE_{redox} / V[b)]	$h\nu_{CT}$ / eV
$[Fe(Cp^*)_2]$	F_4BQ	–0.08[c)]	0.02[e, f)]	–0.10	1.59
	Cl_4BQ	–0.08	0.05[g)]	–0.13	1.60
	Br_4BQ	–0.08	0.00[h)]	–0.18	1.59
	Cl_2BQ	–0.08	–0.18[h)]	0.10	1.60
$[Fe(C_5HMe_4)_2]$	F_4BQ	–0.04[c)]	0.02	–0.06	1.66
	Cl_4BQ	–0.04	0.05	–0.09	1.64
	Br_4BQ	–0.04	0.00	–0.04	1.65
	Cl_2BQ	–0.04	–0.18	0.14	1.64
$[Co(Cp^*)_2]$	F_4BQ	–1.47[d)]	0.02	–1.45	2.14[i)]
	Cl_4BQ	–1.47	0.05	–1.52	2.66[i)]
	Br_4BQ	–1.47	0.00	–1.47	2.48[i)]
	Cl_2BQ	–1.47	–0.18	–1.65	2.10[i)]

[a)] Half-wave redox potentials of donors (E_D) and acceptors (E_A) vs. SCE in CH_3CN, [b)] ΔE_{redox} / V = $E_D - E_A$, [c)] ref. 25, [d)] ref. 26, [e)] ref. 27, [f)] Potentials referenced to SCE, [g)] ref. 28, [h)] ref. 29, [i)] shoulder.

Table 4. Redox potentials of the components and CT energies of ferrocene-based CT complexes.

Complex	E_D / V[a)]	E_A / V[a)]	ΔE_{redox} / V[b)]	$h\nu_{CT}$ / eV
$[Fe(Cp^*)_2]$[Cl_2-naphthoquinone] (**1**)	–0.08[h)]	–0.45[i)]	0.37	1.98
$[Fe(Cp^*)_2]$[Br_2-naphthoquinone] (**2**)	–0.08	–0.30[i)]	0.22	1.94
$[Fe(C_5HMe_4)_2]$[Cl_2-naphthoquinone] (**3**)	–0.04[h)]	–0.45	0.41	
$[Fe(Cp^*)_2]$[acenaphthenequinone][c)]	–0.08	–0.98[j, k)]	0.90	1.5–2.0[o)]
$[Fe(Cp^*)_2]$[CN_2-naphthoquinone][d)]	–0.08	0.20[l)]	–0.28	
$[Fe(Cp^*)_2]$[TCNQ] (1-D phase)[e)]	–0.08	0.21[m)]	–0.29	1.41
$[Fe(C_5HMe_4)_2]$[TCNQ][f)]	–0.04	0.21	–0.25	1.43
$[Fe(Cp^*)_2]$[DMDCNQI][g)]	–0.08	0.06[n)]	–0.14	1.83

[a)] Half-wave redox potentials of donors (E_D) and acceptors (E_A) vs. SCE in CH_3CN except for acenaphthenequinone, [b)] ΔE_{redox} / V = $E_D - E_A$, [c)] ref. 17a, [d)] ref. 18a, [e)] ref. 14, [f)] ref. 15, [g)] ref. 16, [h)] ref. 25, [i)] ref. 30, [j)] ref. 31, [k)] Potentials referenced to SCE in DMF, [l)] ref. 32, [m)] ref. 33, [n)] ref. 34, [o)] broad, ref. 14a.

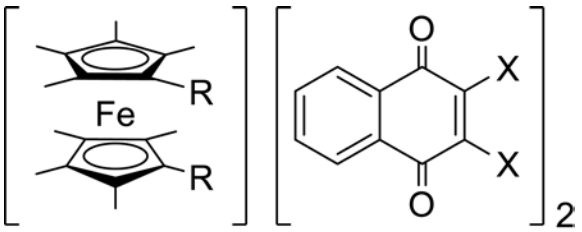

1: R = Me, X = Cl
2: R = Me, X = Br
3: R = H, X = Cl

Fig. 1

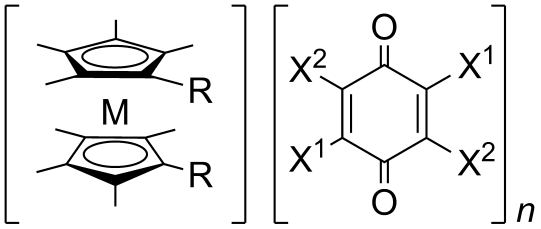

M = Fe, Co
R = Me, H

F_4BQ: $X^1 = X^2 = F$
Cl_4BQ: $X^1 = X^2 = Cl$
Br_4BQ: $X^1 = X^2 = Br$
Cl_2BQ: $X^1 = Cl$, $X^2 = H$

Fig. 2.

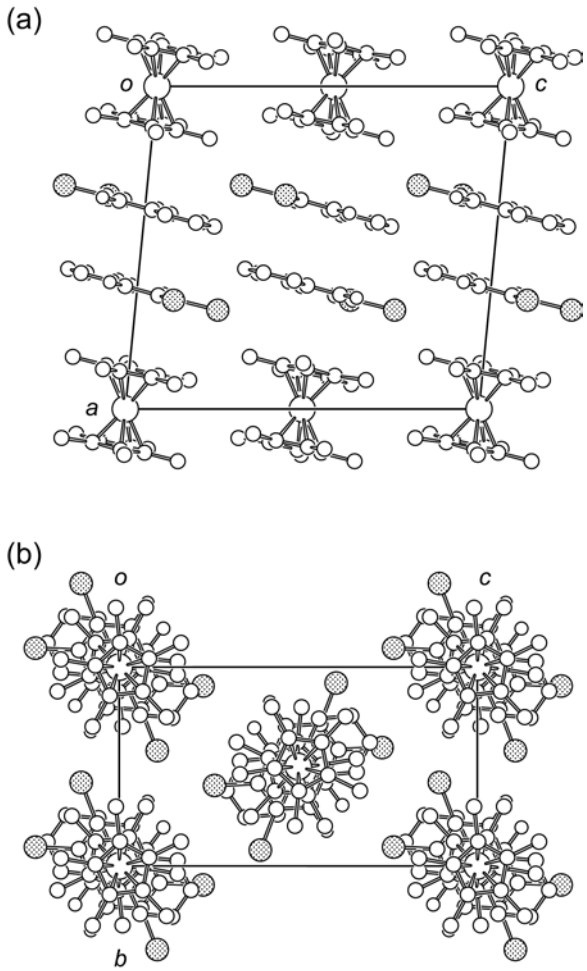

Fig. 3

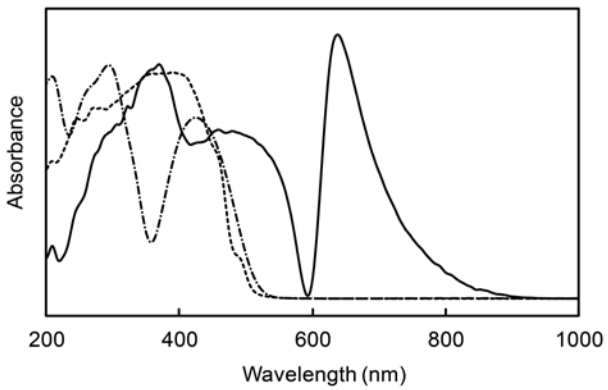

Fig. 4

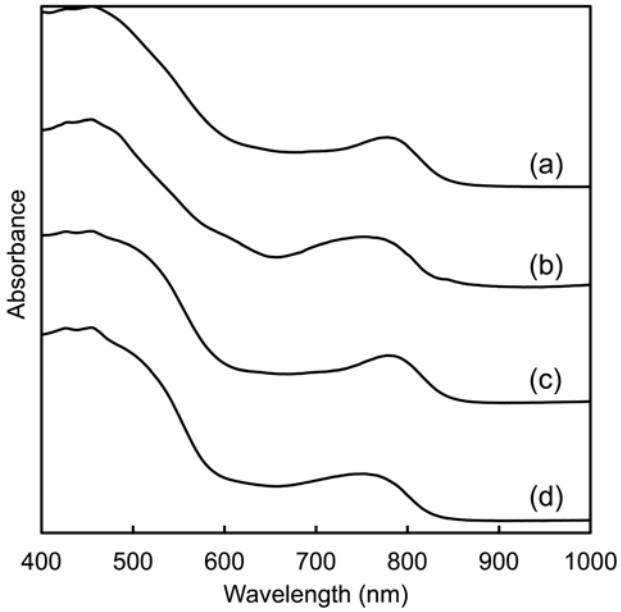

Fig. 5

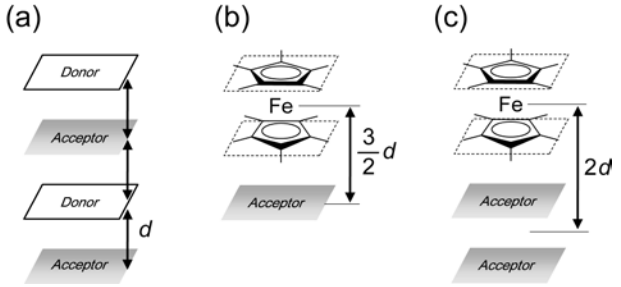

Fig. 6

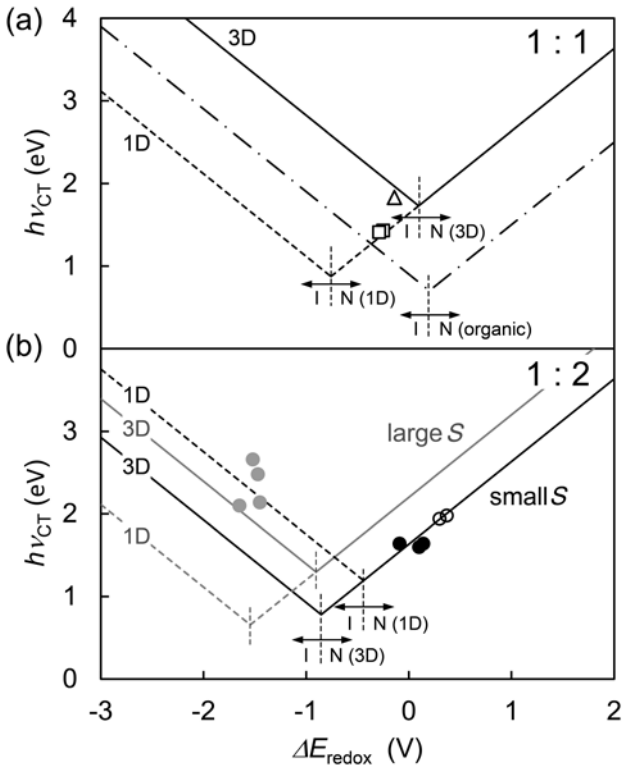

Fig. 7

References

(1) A. Togni and T. Hayashi, Eds., *Ferrocenes: Homogenous Catalysis, Organic Synthesis, Materials Science*, Wiley–VCH: Weinheim, 1995, Chapter 8, and references therein.

(2) D. de Caro, C. Faulmann and L. Valade, *Chem. Eur. J.*, 2007, **13**, 1650.

(3) J. S. Miller, A. J. Epstein and W. M. Reiff, *Angew. Chem., Int. Ed. Engl.*, 1994, **33**, 385.

(4) (a) J. S. Miller, *J. Mater. Chem.*, 2010, **20**, 1846; (b) V. Gama, and M. Almeida, *Top. Organomet. Chem*., 2009, **27**, 97.

(5) J. S. Miller, J. C. Calabrese, H. Rommelmann, S. R. Chittipeddi, J. H. Zhang, W. M. Reiff and A. J. Epstein, *J. Am. Chem. Soc.*, 1987, **109**, 769.

(6) (a) D. Bellamy, N. G. Connelly, G. R. Lewis and A. G. Orpen, *CrystEngComm*, 2002, **4**, 51; (b) M. Fettouhi, L. Ouahab, M. Hagiwara, E. Codjovi, O. Kahn, H. Constant-Machado and F. Varret, *Inorg. Chem.*, 1995, **34**, 4152; (c) Md. B. Zaman, M. Tomura and Y. Yamashita, *Inorg Chim Acta*, 2001, **318**, 127.

(7) (a) T. Mochida, T. Koinuma, T. Akasaka, M. Sato, Y. Nishio, K. Kajita, and H. Mori, *Chem. Eur. J*., 2007, **13**, 1872; (b) T. Mochida, K. Takazawa, H. Matsui, M. Takahashi, M. Takeda, M. Sato, Y. Nishio, K. Kajita and H. Mori, *Inorg. Chem.*, 2005, **44**, 8628; (c) T. Mochida, K. Takazawa, M. Takahashi, M. Takeda, Y. Nishio, M. Sato, K. Kajita, H. Mori, M. M. Matsushita and T. Sugawara, *J. Phys. Soc. Jpn*., 2005, **74**, 2214.

(8) A. Quazi, W. M. Reiff and R. U. Kirss, *Hyperfine Interact*., 1994, **93**, 1597.

(9) (a) J. B. Torrance, J. E. Vazquez, J. J. Mayerle and V. Y. Lee, *Phys. Rev. Lett*., 1981, **46**, 253; (b) J. B. Torrance, A. Girlando, J. J. Mayerle, J. I. Crowley, V. Y. Lee, P. Batail, and S. J. LaPlaca *Phys. Rev. Lett.*, 1981, **47**, 1747.

(10) S. Horiuchi, T. Hasegawa and Y. Tokura, *J. Phys. Soc. Jpn*., 2006, **75**, 051016.

(11) G. Saito and Y. Yoshida, *Bull. Chem. Soc. Jpn.*, 2007, **80**, 1.

(12) (a) A. Arrais, E. Diana, R. Gobetto, M. Milanesio, D. Viterbo and P. L. Stanghellini, *Eur. J. Inorg. Chem.*, 2003, 1186; (b) W. C. Wan, X. Liu, G. M. Sweeney and W. E. Broderick, *J. Am. Chem. Soc.*, 1995, **117**, 9580; (c) P. D. W. Boyd, P. Bhyrappa, P. Paul, J. Stinchcombe, R. Bolskar, Y. Sun and C. A. Reed, *J. Am. Chem. Soc.*, 1995, **117**, 2907; (d) D. V. Konarev. S. S. Khasanov. A. Otsuka and G. Saito, *J. Am. Chem. Soc*., 2002, **124**, 8520.

(13) G. Saito, T. Teramoto, A. Otsuka, Y. Sugita, T. Ban, M. Kusunoki and K. Sakaguchi, *Synth. Met*., 1994, **64**, 359.

(14) J. S. Miller, J. H. Zhang, W. M. Reiff, D. A. Dixon, L. D. Preston, A. H. Reis, E. Gebert, M. Extine, J. Troup, A. J. Epstein and M. D. Ward, *J. Phys. Chem*., 1987, **91**, 4344.

(15) J. S. Miller, D. T. Glatzhofer, D. M. O'Hare, W. M. Reiff, A. Chakraborty and A. J. Epstein, *Inorg. Chem*., 1989, **28**, 2930.

(16) S. Rabaça, R. Meira, L. C. J. Pereira, M. T. Duarte and V. Gama, *J. Organomet. Chem.* 2001, **632**, 67.

(17) (a) H. Nakamura, D. Kuwahara and T. Mochida, *J. Phys. Chem. A*, 2009, **113**, 13601; (b) T. Mochida and K. Yoza, *J. Organomet. Chem.*, 2010, **695**, 1749.

(18) (a) G. T. Yee, M. J. Whitton, R. D. Sommer, C. M. Frommen and W. M. Reiff, *Inorg. Chem*., 2000, **39**, 1874; (b) B. B. Kaul, B. C. Noll and G. T. Yee, *J. Solid State Chem.*, 2001, **159**, 420.

(19) D. P. Freyberg, J. L. Robbins, K. N. Raymond and J. C. Smart, *J. Am. Chem. Soc*., 1979, **101**, 892.

(20) Y. T. Struchkov, V. G. Andrianov, T. N. Sal'nikova, I. R. Lyatifov and R. B. Materikova, *J. Organomet. Chem.*, 1978, **145**, 213.

(21) I. Ikemoto, K. Yakushi, Y. Naito and H. Kuroda, *Acta Cryst*., 1977, **B33**, 2076.

(22) P. M. Breton-lacombe, *Acta Cryst*., 1967, **23**, 1031.

(23) (a) N. Shan, F. Toda and W. Jones, *Chem. Commun*., **2002**, 2372; (b) T. Friščić, A. V. Trask, W. Jones and W. D. S. Motherwell, *Angew. Chem. Int. Ed*., 2006, **45**, 7546; (c) D. Braga and F. Grepioni, *Angew. Chem. Int. Ed.*, 2004, **43**, 4002; (d) K. Tanaka and F. Toda, *Chem. Rev*., 2000, **100**, 1025; (e) D. R. Weyna, T. Shattock, P. Vishweshwar and M. J. Zaworotko, *Cryst. Growth Des*., 2009, **9**, 1106.

(24) (a) A. O. Patil, D. Y. Curtin and I. C. Paul, *J. Am. Chem. Soc*. 1984, **106**, 348; (b) A. V. Trask and W. Jones, *Top. Curr. Chem.*, 2005, **254**, 41.

(25) S. Fukuzumi, H. Kotani, T. Suenobu, S. Hong, Y. -M. Lee and W. Nam, *Chem. Eur. J.*, 2010, **16**, 354.

(26) J. L. Robbins, N. Edelstein, B. Spencer and J. C. Smart, *J. Am. Chem. Soc.*, 1982, **104**, 1882.

(27) C. Frontana, Á. Vázquez, J. Garza, R. Vargas and I. González, *J. Phys. Chem. A*, 2006, **110**, 9411.

(28) C. Vazquez, J. C. Calabrese, D. A. Dixon and J. S. Miller, *J. Org. Chem.*, 1993, **58**, 65.

(29) S. Fukuzumi, S. Koumitsu, K. Hironaka and T. Tanaka, *J. Am. Chem. Soc.*, 1987, **109**, 305.

(30) I. Amada, M. Yamaji, M. Sase, H. Shizuka, T. Shimokage and S. Tero-Kubota, *Res. Chem. Intermed.*, 1998, **24**, 81.

(31) A. Ohashi, T. Aida and J. Tsunetsugu, *J. Mol. Struct.*, 1994, **324**, 75.

(32) M. R. Bryce, S. R. Davies, M. Hasan, G. J. Ashwell, M. Szablewski, M. G. B. Drew, M. Short and M. B. Hursthouse, *J. Chem. Soc., Perkin Trans.*, 1989, **2**, 1285.

(33) F. Marken and R. G. Compton, *Ultrason. Sonochem.*, 1996, **3**, S131.

(34) S. L. Schiavo, G. Bruno, P. Zanello, F. Laschi and P. Piraino, *Inorg. Chem.*, 1997, **36**, 1004.

(35) T. Mochida, K. Okazawa and R. Horikoshi, *Dalton. Trans*., 2006, 693.

(36) Y. Funasako, T. Mochida, T. Sakurai and H. Ohta, *J. Organomet. Chem.* 2011, **696**, 2621.

(37) (a) T. Mori, A. Kobayashi, Y. Sasaki, H. Kobayashi, G. Saito and H. Inokuchi, *Bull. Chem. Soc. Jpn*., 1984, **57**, 627; (b) T. Mori, Energy band calculation software package. See http://www.op.titech.ac.jp/lab/mori/lib/program.html.

(38) A. Anmüller and S. Hünig, *Liebig Ann. Chem.*, 1986, **142**, 165.

(39) G. M. Sheldrick, *SHELXL: Program for the Solution for Crystal Structures*, University of Göttingen, Germany, 1997.

(40) G. M. Sheldrick, *SADABS: Program for Semi-empirical Absorption Correction*, University of Göttingen, Germany, 1997.

(41) L. J. Farrugia, *ORTEP-3 for Windows, J. Appl. Cryst.*, 1997, **30**, 565.

Supplementary information

Charge-transfer Complexes from Decamethylferrocene and 1,4-Quinone Derivatives — Neutral–ionic Phase Diagrams for Metallocene Complexes

Tomoyuki Mochida,* Yusuke Funasako and Hiroko Azumi

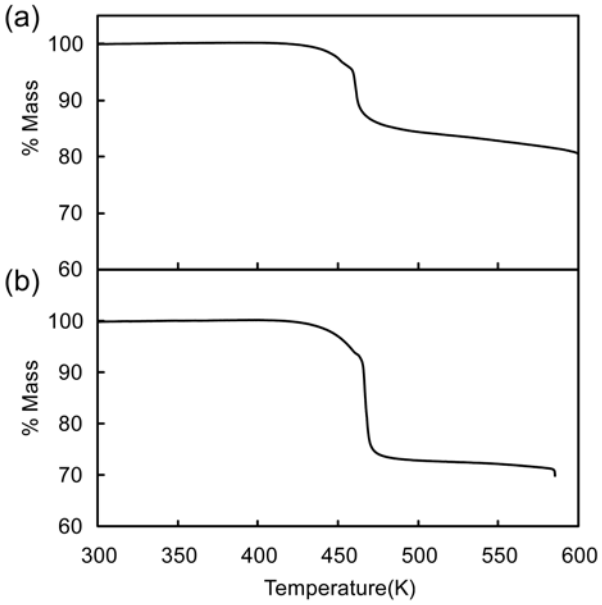

Fig. S1. TG traces of (a) **1** and (b) **2**.

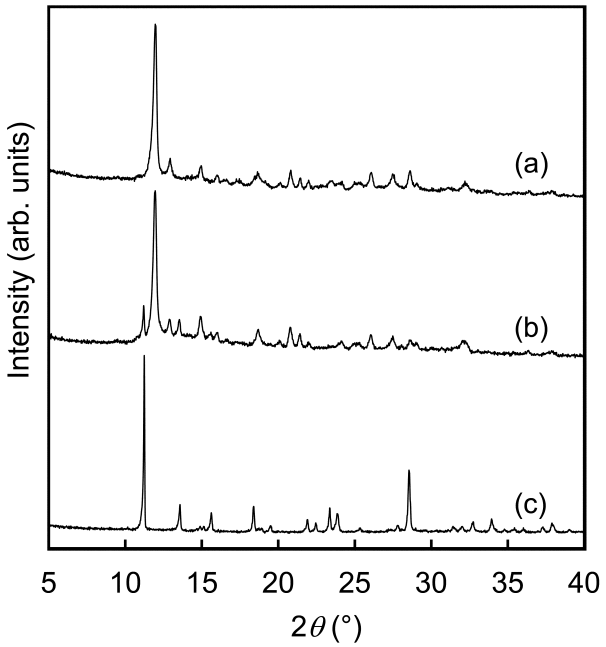

Fig. S2. XRD patterns of powders obtained by ball-milling of [Fe(C_5HMe_4)$_2$] and Cl_2BQ in the presence of a drop of dichloromethane in DA ratios of (a) 1:2 and (b) 1:1. (c) XRD pattern of a mixture of [Fe(C_5HMe_4)$_2$] and Cl_2BQ.

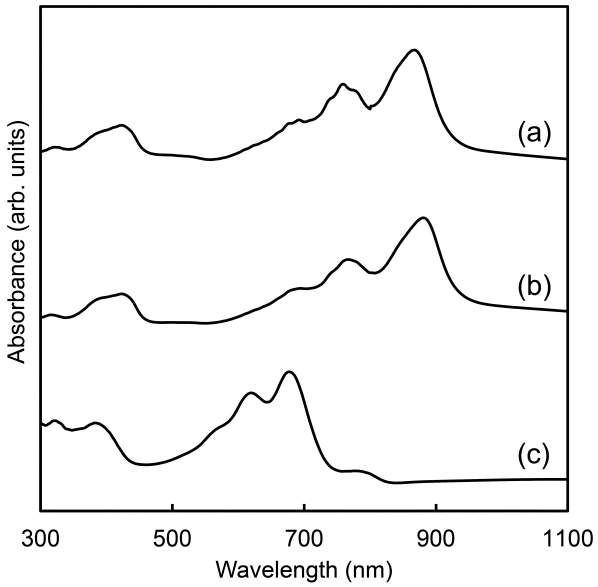

Fig. S3. Solid-state electronic spectra of (a) $[Fe(Cp^*)_2][TCNQ]$, (b) $[Fe(C_5HMe_4)_2][TCNQ]$, and (c) $[Fe(Cp^*)_2][DMDCNQI]$.

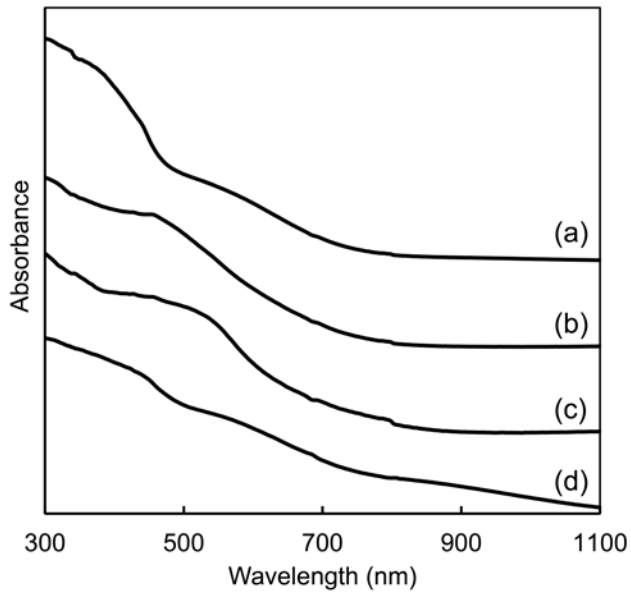

Fig. S4. Solid-state electronic spectra of the reaction products of $[Co(Cp^*)_2]$ and (a) F_4BQ, (b) Cl_4BQ, (c) Br_4BQ, and (d) Cl_2BQ.

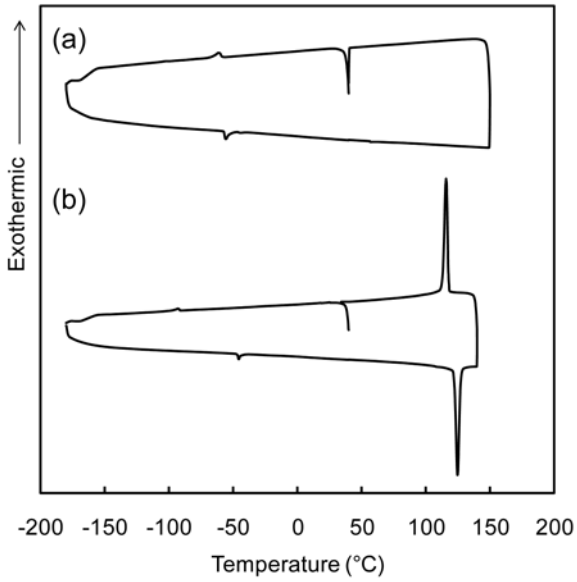

Fig. S5. DSC traces for (a) $[Fe(Cp^*)_2][TCNQ]$ (1-D phase) and (b) $[Fe(C_5HMe_4)_2][TCNQ]$.